Transient Stability Analysis of the Ecuadorian Electrical System: Case of the Southern Segment

DARWIN PILA, CARLOS QUINATOA, LUIS CAMACHO, JIMMY VACA
Department of Electrical Engineering,
University Technical of Cotopaxi,
Av. Simón Rodríguez s/n Barrio El Ejido Sector San Felipe,
Latacunga,
ECUADOR

Abstract: - The study aims to identify and assess the risks related to possible disturbances and contingencies within the National Interconnected System (SNI). Technical aspects are analyzed to determine the system's capacity to recover quickly from such events and maintain the continuity of power supply in a safe manner. For this purpose, an SNI network, composed of generators, transformers, transmission lines and loads, has been chosen using data from institutions of the Ecuadorian electricity sector. The study followed a progression that encompassed data collection, power network modeling, model verification, study scenarios, transient stability simulations and analysis of results. Three cases were studied: steady state simulation, three-phase fault in the transmission line between node 1 and 11, and opening of the Termogas Machala Generator. The results showed that the lines connecting the Milagro 230 kV bus and CNEL Guayas - The Ríos are at 83.5% of their total load, causing congestion and a low voltage level of 0.9057 pu, close to the lower limit. At node 8 (CNEL The Oro), the voltage level is 0.95443 pu, adequate for the load supplied. Except at node 12 (Peru generator), the variations of P and Q, as well as voltage and angle, stabilize quickly at all nodes. At node 12, these variables show greater variation and take longer to stabilize.

Key-Words: - System, Interconnected, Generators, Lines, Analysis.

Received: May 25, 2024. Revised: August 19, 2024. Accepted: September 11, 2024. Published: October 29, 2024.

1 Introduction

Ecuador's National Interconnected System (SNI) is a network that consolidates several segments to guarantee a continuous and reliable supply of electricity throughout the country. Each segment of the system plays a fundamental role in the dispersion and transport of electrical energy, which is indispensable for the efficient operation of the entire system. Within this framework, transient stability presents itself as a crucial element that requires specialized knowledge to ensure the safe and efficient operation of each segment.

Transient stability analysis in Ecuador involves assessing the ability of the power system to maintain synchronous operation after a disturbance. Research conducted in Ecuador has focused on the replication of the Ecuadorian power system in real-time simulation platforms such as HyperSim, [1], along with the incorporation of wind generation to adjust system operating points and evaluate stability before and after wind farm integration, [2]. In addition, research has highlighted the importance of transient stability in future power grid scenarios by analyzing variables that influence genset stability and effective mitigation measures, [3]. In addition, evidence has been presented showing that the deployment of flexible alternating current transmission systems (FACTS) improves stability, reduces losses and increases system load carrying capacity and methodologies such as the equal-area criterion are applied to analyze stability with and without FACTS devices under various fault conditions, [4]. Taken together, these investigations improve a comprehensive understanding of transient stability in the Ecuadorian power system.

For an accurate assessment of transient stability, it is crucial to use dynamic models that describe the characteristics of synchronous machines, generators and other critical elements of the power grid. These models make it possible to simulate the dynamic response of the system to various operating conditions, which speeds up the analysis of its reaction to disturbances and the identification of areas requiring improvement.

Considering that transient stability is essential in the operation of power systems, as it is dedicated to evaluate the ability of the system to maintain synchronism after a disturbance. Several methodologies and resources have been designed for the examination of transient stability, including Dynamic Computation for Power Systems (DCPS) software for system simulations, [5], reachability analysis to confirm the stability of transient responses, and an ensemble-based approach

using barrier theory to identify acceptable ensembles and robust invariant ensembles to assess the transient stability characteristics of power systems, [6]. These evaluations typically involve collecting generator operating data, establishing characteristic ellipsoids, scrutinizing transient energy functions and calculating the critical clearing time (TccT) to determine system stability and guide decision-making procedures in power system governance and design, [7], [8].

Transient stability is then essential in electric power systems to maintain synchronization between generators during disturbances. Proactive measures, such as optimization of power flow models like TSC-OPF, are implemented to preemptively adjust system parameters and improve stability, [9]. In the event of a contingency, reactive strategies, such as load reduction, are activated after a disturbance to avoid further instability, [10]. Research on networks, such as the IEEE 9-bus and Western System Council Coordinator (WSCC) systems incorporating renewable energy, highlights the influence of disturbances on stability and the effectiveness of devices such as the automatic voltage regulator (AVR) and power system stabilizer (PSS) in enhancing transient stability, [11]. Innovative approaches, such as the use of neural networks for visual attention, improve the assessment of transient stability by considering the topology of the power grid and refining model interpretation, [12]. Transient stability is essential to ensure the safe and reliable operation of power systems under conditions of disturbances and outages.

This requires ensuring the reliability and operational safety of the power system. As demand grows and technology advances, it is crucial to anticipate and mitigate the risks associated with temporary events that could threaten continuous and reliable operation. As a result, the study is expected to provide valuable information for system operators, planners regulators and enable them to make informed decisions to improve and strengthen the segment in question. Accordingly, the study is expected to identify potential improvements, assess the system's responsiveness to disturbances, and propose corrective measures to improve its resilience and reliability, [13].

For the purpose, the transient stability of a particular segment of the SNI is crucial to ensure a reliable and safe electricity supply. Through a thorough and comprehensive assessment, it aims to improve the power grid, minimize hazards and maintain the level of electricity supply to consumers.

2 SNI Technical Data in the Face of Disturbances and Transient Events

The study of transient stability is crucial to ensure the safe and reliable operation of interconnected power grids. In the context of Ecuador's SNI, the current research focuses on analyzing a particular segment to evaluate its dynamic performance when exposed to temporary disturbances and incidents. This comprehensive methodology outlines the suggested approach to carry out such analysis, delving into crucial elements such as the necessary information, the minimum system configuration, the dynamic simulations, the expected results and the limitations of the research.

2.1 Dynamic Models for Generators

Dynamic models intended for use in the electrical system shall be classified as follows:

- Machine model;
- Exciter model;
- Speed governor model.

To achieve this objective, the parameters supplied by CENACE and CELEC EP Transelectric will be used, as described in [14].

2.1.1 Machine Model

The models intended for use will align with the frameworks defined in IEEE standards and are suitable for generators located within the power system model. These models are included in the PowerWorld libraries.

The initial model corresponds to the (GENROU) machine model known as Solid Rotor Generator, which is characterized by the inclusion of a rotor with equal mutual inductance. This model provides a very accurate representation of the behavior exhibited by a synchronous generator in the specific dynamics being examined within a transient stability analysis up to 10 Hz. It is specifically designed to represent a solid rotor machine equipped with three damping coils. It should be noted that more than two-thirds of the generators included in the Eastern North American Interconnection (MMWG) framework are represented with this particular model. The parameters and values assigned to this model are aligned with the standard values built into the software, allowing customization of individual generators. This model is designed to be applied to most generating units, except for the Zorritos bus and Milagro bus 230 kV generators, which will follow a design based on the classical model concept.

The schematic diagram associated with this model is as follows Figure 1.

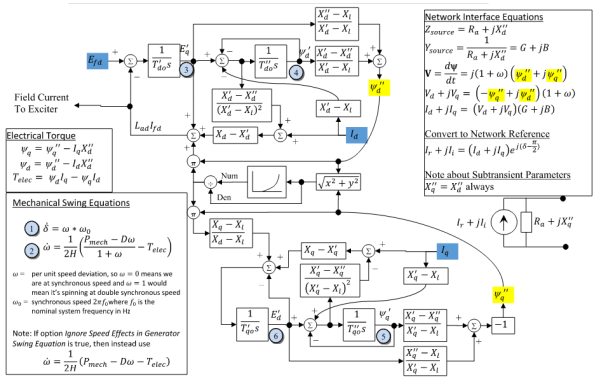

Fig. 1: GENROU block diagram [15]

The generators located at the Milagro and Zorritos 230 kV bus bars correspond to equivalent generators. Although they do not physically exist, they are represented as an equivalent to allow the Milagro bus to function as a slack or floating bus. In addition, the Zorritos bus is modeled for interconnection with Peru. The GENCLS_PLAYBACK, [16], machine model will be applied to these two equivalent generators. This model is a synchronous machine model that uses a classical model or a Thevenin voltage source to reproduce the voltage or frequency. This configuration is shown in Figure 2.

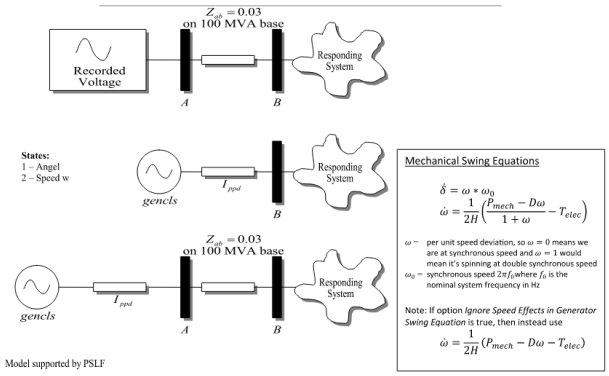

Fig. 2: Schematic of GENCLS_PLAYBACK [15]

2.1.2 Excitation Systems

An excitation system, or excitation control system, is a set of devices created to provide and regulate the generator field current through automatic regulators, allowing voltage control. The selection of the models to be used, as described below, is based on the principles established in reference, [14].

The generators associated with Hidrosibimbe, Hidrotambo and Zorritos will be analyzed using the SEXS model, [13], based on factors such as rated capacity, technology and operating status. This model in Figure 3, provides a simplified representation of the excitation system in a block diagram format.

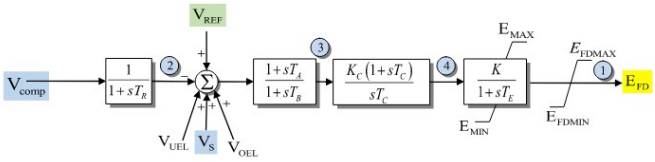

Fig. 3: SEXS block diagram [17]

The input parameters provided are aligned with the following,in Figure 4.

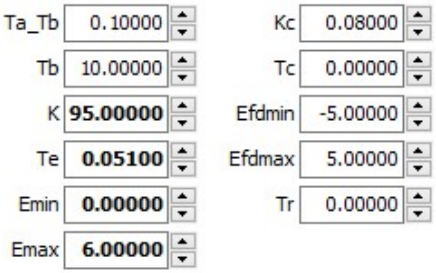

Fig. 4: Parameters for the SEXS block diagram [17]

In contrast, Termo Gas Machala will use the EXAC1 model, specifically an IEEE AC1 type excitation system model, as shown in the block diagram in Figure 5.

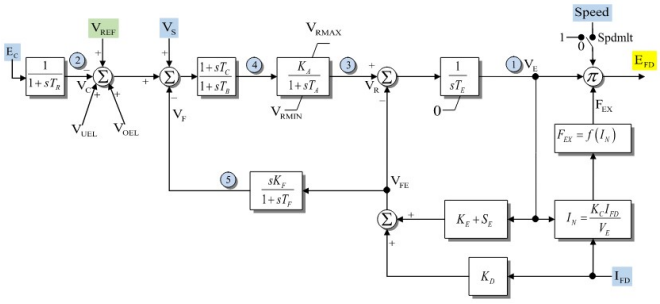

Fig. 5: EXAC1 block diagram [17]

The parameters entered correspond to the following, in Figure 6.

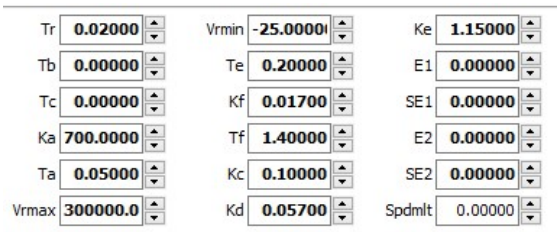

Fig. 6: Parameters for the EXAC1 block diagram [17]

For the Minas San Francisco power plant, the EXST3 model will be used, specifically the IEEE excitation system model type ST3, [18], as shown in Figure 7.

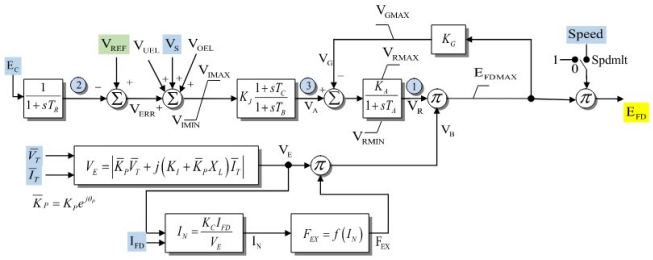

Fig. 7: EXST3 block diagram [17]

The parameters entered correspond to the following, in Figure 8.

Tr	0.03000	Ta	0.40000	Kc	0.10400
ViMax	0.20000	Vrmax	1.00000	Xl	0.01510
ViMin	-0.20000	Vrmin	0.00000	VgMax	6.25000
Kj	200.00000	Kg	1.00000	ThetaPDeg	0.00000
Tc	1.00000	Kp	3.35000	Spdmlt	0.00000
Tb	10.00000	Ki	0.00140		
Ka	20.50000	Efdmax	3.02000		

Fig. 8: EXST3 block diagram parameters [17]

In contrast, the equivalent generator located at the slack bar will employ the EXPIC1 model, which indicates an integral/proportional excitation system model, as shown in the block diagram in Figure 9.

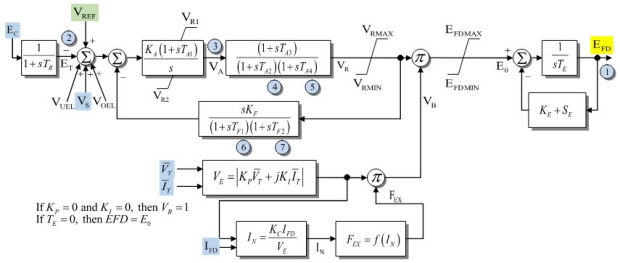

Fig. 9: EXPIC1 block diagram [17]

The parameters entered correspond to the following, in Figure 10.

Tr	0.00000	Vrmax	99.00000	Te	0.00000
Ka	9.30000	Vrmin	-99.00000	E1	0.00000
Ta1	3.80000	Kf	0.00000	SE1	0.00000
Vr1	4.90000	Tf1	1.00000	E2	0.00000
Vr2	-3.00000	Tf2	0.00000	SE2	0.27000
Ta2	0.02800	Efdmax	99.00000	Kp	0.00000
Ta3	0.00000	Efdmin	-99.00000	Ki	0.00000
Ta4	0.02900	Ke	0.00000	Kc	0.00000

Fig. 10: EXPIC1 block diagram parameters [17]

2.1.3 Speed Regulation Systems

The speed of a generator is normally controlled by a governor, which comprises a speed regulation mechanism commonly known as a governor. This device uses mechanical, hydraulic or electronic methods to autonomously maintain the rotor speed within a specific range. The main function of this control device is to identify any discrepancy in motor speed and quickly restore it to its optimum level, thus ensuring frequency stability in the power grid. The selection of the models described below was based on the guidelines described in, [14].

For the generators associated with the Milagro and Zorritos projects, it is proposed to use the IEEEG1 type 1 turbine governor model, based on their operating characteristics and technological requirements. The schematic representation of this model can be seen in Figure 11.

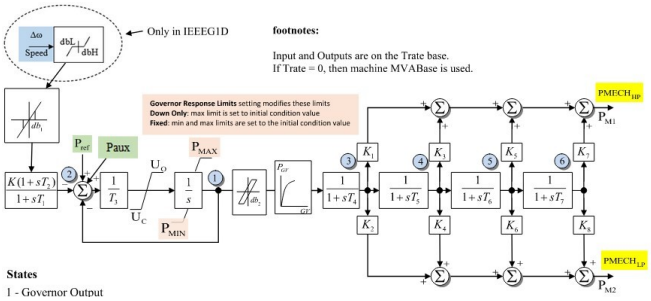

Fig. 11: Block diagram of IEEEG1 [17]

The parameters entered correspond to the following, in Figure 12, this part details the data entered from IEEEG1 in order to be able to validate:

K	14.27000	K1	0.00000	K7	0.00000	Gv3	0.00000
T1	0.30000	K2	1.00000	K8	0.00000	Pgv3	0.00000
T2	0.00000	T5	0.00000	db1	0.00000	Gv4	0.00000
T3	0.18000	K3	0.00000	Eps	0.00000	Pgv4	0.00000
Uo	0.10000	K4	0.00000	db2	0.00000	Gv5	0.00000
Uc	-0.10000	T6	0.00000	Gv1	0.00000	Pgv5	0.00000
Pmax	1.00000	K5	0.00000	Pgv1	0.00000	Gv6	0.00000
Pmin	0.00000	K6	0.00000	Gv2	0.00000	Pgv6	0.00000
T4	0.40000	T7	0.00000	Pgv2	0.00000	Trate	0.00000

Fig. 12: Parameters for the block diagram of IEEEG1 [17]

For Hidrosibimbe, Hidrotambo and Minas San Francisco, the use of the type 3 turbine governor model (IEEE 1981) IEEEG3, [16], [18], will depend on the specific type of Pelton turbine and its corresponding technology. This model serves as a simplified representation of the excitation system and is shown in the block diagram in Figure 13. This model is widely recognized and well documented, demonstrating its effectiveness in the simulation and analysis of hydroelectric generation systems.

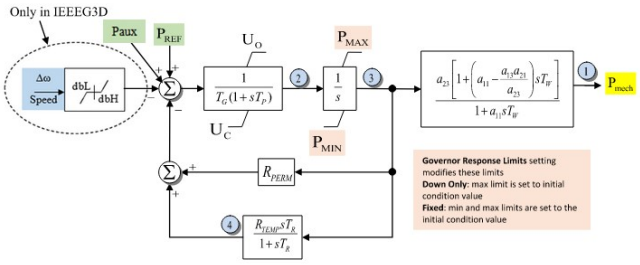

Fig. 13: Block diagram of IEEEG3 [17]

The parameters entered correspond to the following Figure 14.

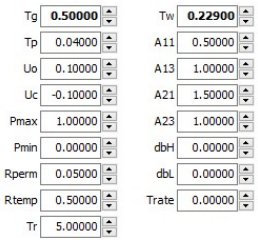

Fig. 14: IEEEG3 Block Diagram Parameters [17]

In addition, the GASTD gas turbine regulator model will be used for Thermo Gas Machala, as demonstrated in the block diagram shown in Figure 15.

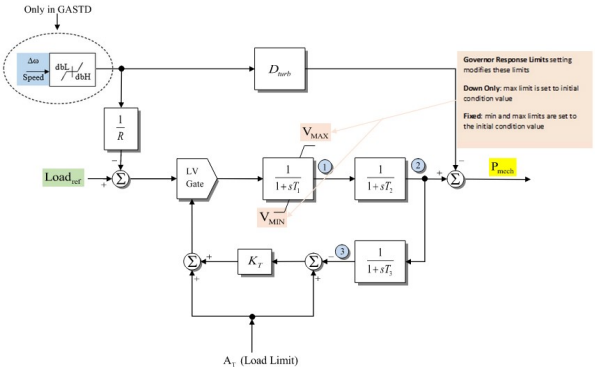

Fig. 15: GASTD block diagram [17]

The parameters entered correspond to the following Figure 16:

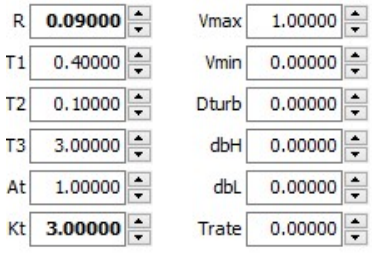

Fig. 16: GASTD block diagram [17]

2.2 Electrical System Technical Data

To analyze the data, information obtained from the official websites of the National Electricity Operator (CENACE), [19], and the Agency for Regulation and Control of Energy and Non-Renewable Natural Resources was used, and the latter adhered to the parameters described in the statistics, [20], and the geo-portal, [21].

To establish an accurate electrical model, the methodology initially aims to determine the load power values. In this scenario, information extracted from statistical data from the electricity sector is used. By considering the monthly energy consumption of the loads shown in the one-line diagram and adjusting it for the evaluation period, the average active power is obtained. It is crucial to maintain a power factor of at least 0.92, [22], at the connection points between the distributor and the SNI. Consequently, the reactive power can be calculated . The results of these calculations are shown in Table 1.

Table 1. Determination of the load of the modeled electrical system

Load (CNEL)	Energy - Jan 2024 (MWh)	Energy - Feb 2024 (MWh)	Medium Energy (MWh)	Active Power (MW)	Reactive Power (MVAr)
Guayas - Los Ríos	306,694.61	300,994.94	303,844.77	422	180
Milagro	89,983.94	92,279.78	91,131.86	127	54
Los Ríos	50,893.99	49,592.13	50,243.06	70	30
EL Oro	151,761.59	145,843.09	148,802.34	207	88

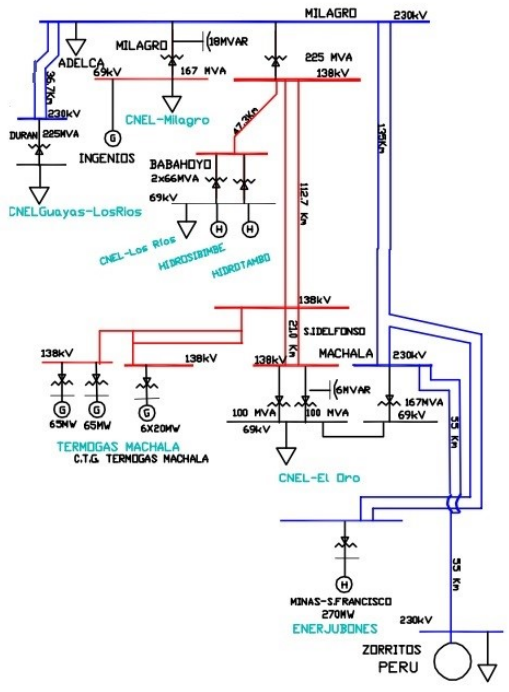

Fig. 17: One-line diagram of the section of the SNI applicable to the study

The configuration of the SNI network segment analyzed corresponds to that found in the southern region of Ecuador, as shown in Figure 17. The load at the Zorritos bus bar is determined based on binational electrical studies. In this particular case, the active power is 40 MW and the reactive power is 17 MVAr.

In addition, the identification of the components or elements of the simulated electrical system has been carried out based on the data specified in the statistics of the electrical sector. The following Table 2, Table 3 and Table 4 show the information related to connections, capacitors and generators. It is important to note that the 230 kV Milagro bus is representative of an infinite bus.

Table 2. Power grid data of the modeled power system

Node *i*	Node *j*	R *(pu)*	X *(pu)*	B *(pu)*	Limit MVA
1	2	0.01938	0.05917	0.0396	300
1	2	0.01938	0.05917	0.0396	300
1	3	0	0.35618	0	180
1	4	0	0.17615	0	225
1	9	0.01811	0.05763	0.0281	450
1	11	0.01695	0.04739	0.0255	300
4	5	0.02701	0.0571	0.026	125
4	6	0.01335	0.04211	0.0096	400
7	6	0.01711	0.0411	0.0241	300
6	8	0.01181	0.0445	0.016	450
8	10	0.01271	0.02704	0.0324	225
9	10	0	0.19207	0	225
9	11	0.01809	0.04999	0.0275	300
9	12	0.01709	0.0348	0.0448	100

Table 3 serves as a valuable tool for operational planning and coordination of generator deployment within an electric power system. It allows optimization of resource utilization based on demand dynamics and operating costs.

Table 3. Modeled power system generator data

Node	Pmax (MW)	Pmin (MW)	B ($/MWh)	Qmax (MVAr)	Qmin (MVAr)
G1/3	78	0	43	58.5	-58.5
G2/5	8	0	2	6	-6
G3/5	16	0	2	12	-12
G4/7	276	0	54	207	-207
G5/11	270	0	2	220	-220
G6/12	60	0	35	45	-45
G7/1	300	0	2	265	-265

Table 4 shows the load data related to the simulated electrical system.

Table 4. Modeled power system load data

Node	Status	MW	MVAr	MVA
2	closed	422	180	458.79
3	closed	127	54	138
5	closed	70	30	76.16
8	closed	207	88	224.93
12	closed	40	17	43.46

The schematic diagram of the simulated system can be seen in Figure 18.

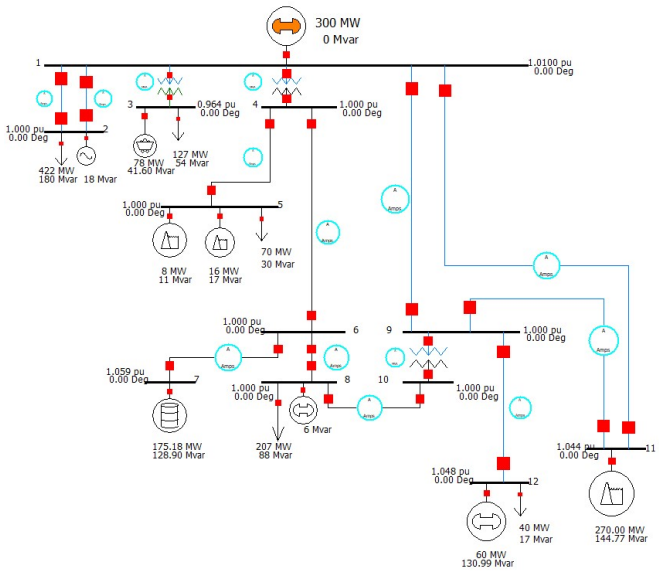

Fig. 18: One-line diagram of the model electrical system

2.3 Case Studies

To carry out the analysis, we will proceed to establish the case studies, as described below:

- Steady state simulation of the system based on the imposed demand:

  This research is carried out by performing a power flow analysis under steady state conditions, with the objective of validating the electrical system and acquiring the electrical parameters.

- Three-phase fault on L/T between node 1 and 11:

  The transmission line connecting the Milagro node to the Minas San Francisco power plant plays a crucial role in the plant's power evacuation process. Therefore, performing an analysis in the event of a line failure and its subsequent opening is critical for the system.

- Opening and reclosing of Termogas Machala Generator:

  In the simulated electrical system, it is evident that the Termogas Machala power plant plays a key role due to the significant amount of energy it provides. Consequently, an abrupt interruption of this facility could cause substantial damage to the system, which underlines the importance of performing a stability analysis in this scenario and its subsequent shutdown after a designated period of time.

3 Modeling of the Electrical System using PowerWorld Software

PowerWorld is used to model the power system and provides essential tools for network planners, power marketers, operators, system builders, educators and others interested in performing power system analysis in an easy-to-use format.

3.1 Steady State Simulation of the System

This initial case study focuses on the electrical validation of the proposed electrical system. To achieve this objective, the electrical model described with PowerWorld was simulated under steady state conditions. The results are detailed in the following Tables in the one-line diagram shown in Figure 19.

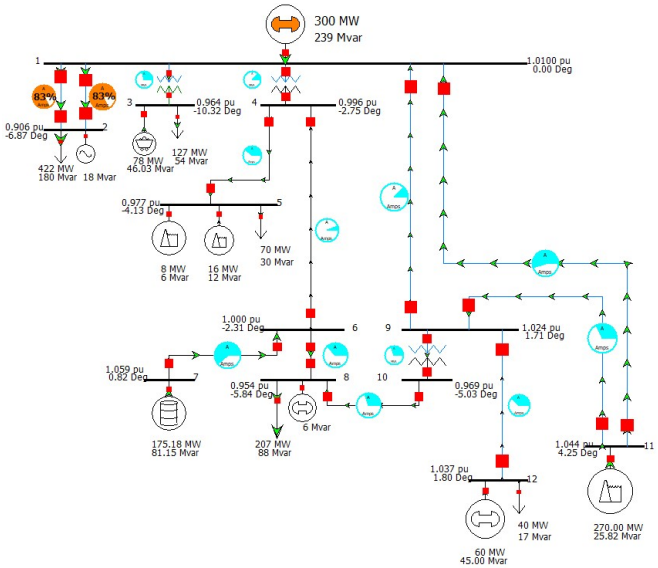

Fig. 19: Power flow of the electrical system

Table 5. Flows in the links

Node *i*	Node *j*	Flow (MW)	Lim (MVA)	Lim % (MVA) (Max)	Loss (MW)
1	2	223	300	83.5	12.01
1	2	223	300	83.5	12.01
1	3	49	180	28.9	0
1	4	27.4	225	12.7	0
1	9	-55.2	450	12.5	0.55
1	11	-167.2	300	57.6	4.65
4	5	46.6	125	38.3	0.63
4	6	-19.2	400	4.9	0.05
7	6	175.2	300	64.4	5.72
6	8	150.2	450	36.5	3.2
8	10	-60	225	29	0.58
9	10	60.6	225	30.6	0
9	11	-96.5	300	32.8	1.61
9	12	-19.8	100	37.9	0.21

The results in Table 5 show that the simulated electrical network facilitates power flow convergence under the following conditions, which confirms the effectiveness of the data and information acquired. Consequently, an observation can be made with respect to the transmission lines linking the Milagro 230 kV substation with CNEL Guayas - Los Rios, which operate at 83.5% of their maximum capacity. Furthermore, it is evident that, due to this congestion, the voltage level has dropped to 0.9057 pu unit, placing it close to the lower threshold.

Similarly, in Table 6, it is observed that node 8 hosts the second most significant load in the simulated electrical network, associated with CNEL El Oro, leading to a voltage increase of 0.95443 pu. This fact can be rationalized if the magnitude of the load requirement is considered. In addition, the presence of other technical factors and electrical parameters indicates compliance with the predefined technical standards in the operation of the electrical network.

Table 6. Results evaluated in the nodes

Node	Nom (kV)	PU (Volt)	Volt (kV)	Ang (Deg)	Load (MW)	Gen (MW)
1	230	1.01	232.3	0	-	300.04
2	230	0.90574	208.321	-6.87	422	0
3	69	0.9642	66.53	-10.32	127	78
4	138	0.99647	137.513	-2.75	-	-
5	138	0.97718	134.852	-4.13	70	24
6	138	1.00048	138.067	-2.31	-	-
7	138	1.0593	146.183	0.82	-	175.18
8	138	0.95443	131.711	-5.84	207	0
9	230	1.02361	235.431	1.71	-	-
10	138	0.96935	133.77	-5.03	-	-
11	230	1.044	240.12	4.25	-	270
12	230	1.03711	238.536	1.8	40	60

3.2 Three-Phase Fault on L/T between Node 1 and 11

To evaluate this event, we used PowerWorld, with the input parameters shown in Figure 20.

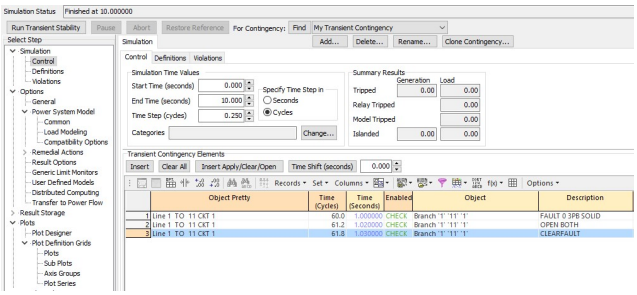

Fig. 20: Event 1 entry in the software

Figure 21 shows the frequency response of two buses, namely bus 4 and bus 5, within an electrical network. An initial disturbance is detected, followed by damped oscillations gradually approaching a constant frequency of around 60 Hz. The behavior of the curves of both buses shows a remarkable

resemblance, suggesting an almost identical reaction to the incident disturbance.

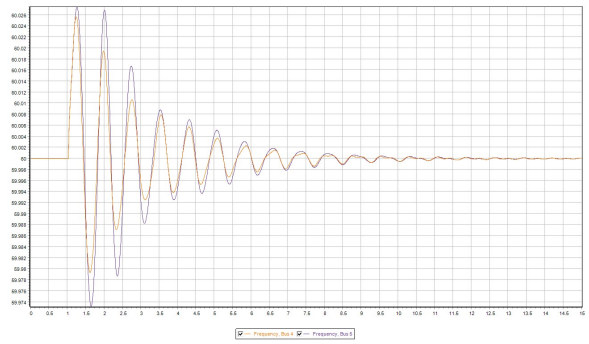

Fig. 21: Frequency at nodes 4 -5

Figure 22 shows the frequency response of three bus 6, bus 7 and bus 8 within an electrical network. After an initial disturbance, damped oscillations occur and converge to a stable frequency of around 60 Hz. The responses of the three buses show almost identical patterns, suggesting a high degree of similarity in their response to disturbances.

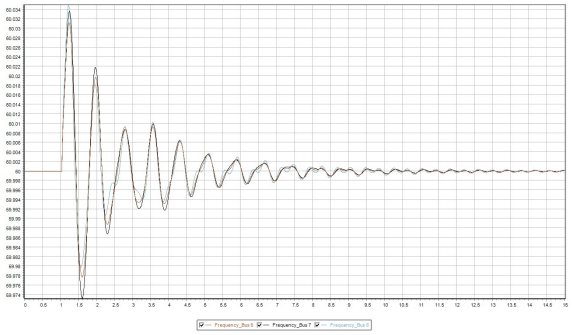

Fig. 22: Frequency in nodes 6 -7 -8

The data show that the most significant frequency variation is observed at the nodes close to the fault (Figure 23). However, after the fault is resolved, the speed controllers perform their function effectively, which significantly reduces the frequency variation at the end of the evaluation period.

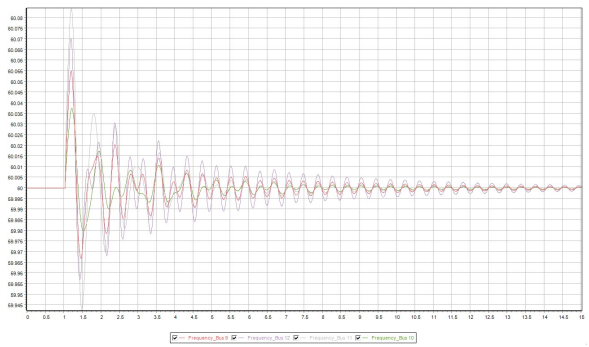

Fig. 23: Frequency at nodes 9 -10 -11-12

In addition, to confirm the operation of the voltage regulators through the drive system, the variations of the voltage levels at the various nodes are shown in Figure 24 below.

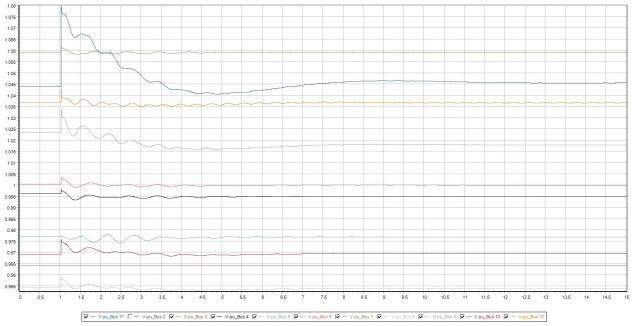

Fig. 24: Node voltages

The Figure shows how the voltage regulators work to stabilize the variation of this electrical parameter over the duration of the analysis, which ensures the efficiency of the exciter models. In the scenario being examined, the voltage variation that occurs at node 11 and thus affects node 9.

The voltage and angle stabilization for each node can be evaluated by referring to Figure 25, Figure 26, Figure 27, Figure 28 and Figure 29.

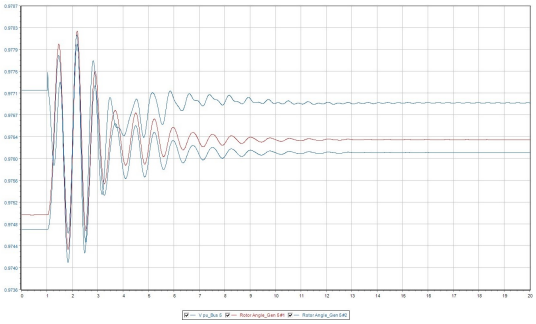

Fig. 25: Voltage and rotor angle variation - node 5

Figure 26 shows the oscillatory behavior of the generator rotor angle 7 and the voltage on bus 7 after a disturbance. Both parameters show damped oscillations that gradually stabilize, reflecting the reaction of the system to the initial disturbance.

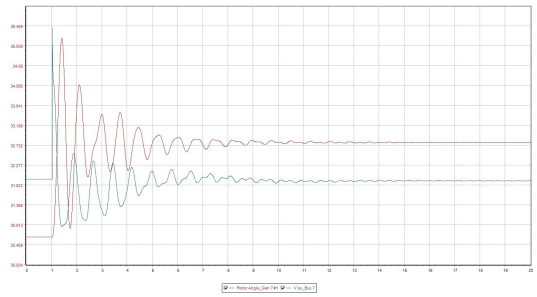

Fig. 26: Voltage variation and rotor angle - node 7

Figure 27 shows the oscillations of the magnitude (in blue) and angle (in red) of voltage on an electrical bus after a disturbance. Both signals exhibit transient behavior that stabilizes after approximately 12 seconds.

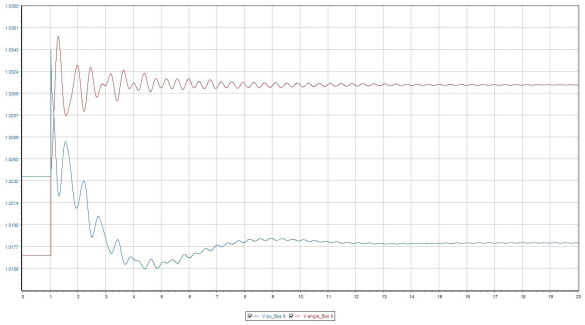

Fig. 27: Voltage variation and rotor angle - node 9

Figure 28 shows the generator rotor angle 11 and the voltage on bus 11 after a disturbance. These variables show initial oscillations that gradually stabilize, showing the progression of the system towards a new equilibrium after the disturbance.

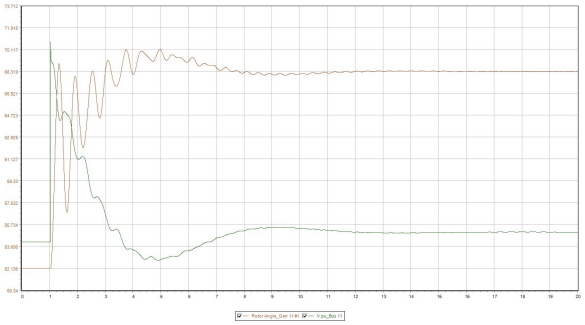

Fig. 28: Voltage variation and rotor angle - node 11

Figure 29 represents the rotor angle of generator 12 and the voltage on bus 12 after a disturbance. Both show damped oscillations gradually approaching a stable equilibrium, which shows the dynamic behavior of the electrical system.

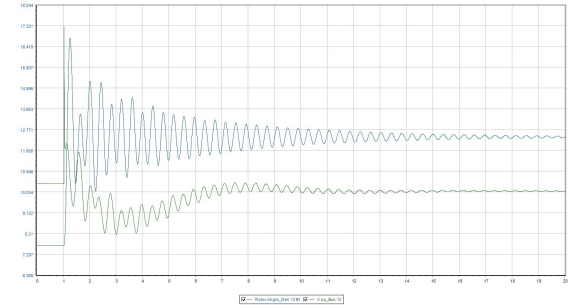

Fig. 29: Voltage variation and rotor angle - node 12

The voltage and angle variations at each node indicate a stabilization of the variables in a pressurized manner, except at node 12. It is noted that at node 12, which houses the Peruvian generator, there is a greater variation, leading to a prolonged stabilization process compared to other nodes.

Finally, the active and reactive power of the generators is evaluated and each generator is shown in Figure 30.

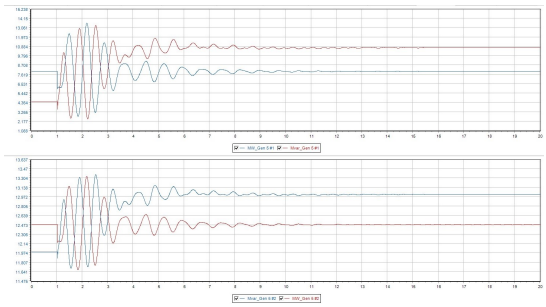

Fig. 30: Variation of P and Q - Generators located at node 5

Figure 31 shows the active (MW) and reactive (Mvar) power oscillations of generator 7 after a disturbance. The curves shown show damped oscillations gradually approaching stable levels, indicating the long-lasting stability of the power system.

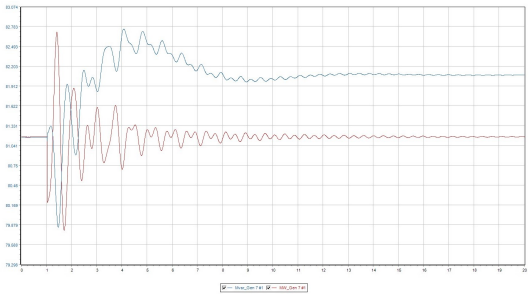

Fig. 31: Variation of P and Q - Generator located at node 7

Figure 32 shows the oscillations of the active power (shown in blue) and reactive power (shown in red) of a generator after a disturbance. Both signals show transient characteristics that finally stabilize after about 12 seconds.

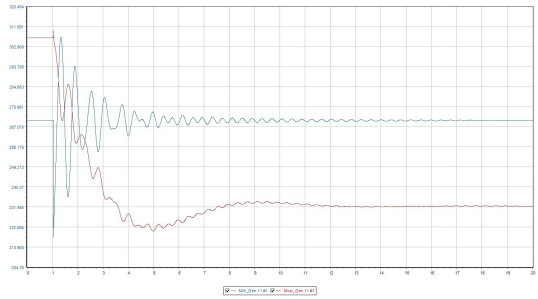

Fig. 32: Variation of P and Q - Generator located at node 11

Figure 33 shows the oscillations of active power (shown in blue) and reactive power (shown in red)

of a stand-alone generator after a disturbance. Both waveforms show transient characteristics with a noticeable frequency that finally stabilizes after about 15 seconds.

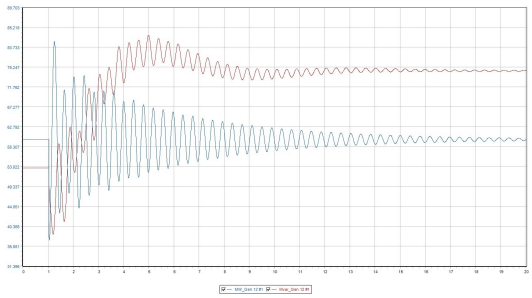

Fig. 33: Variation of P and Q - Generator located at node 12

Similarly, the variations of P and Q at each node indicate that, except at node 12, there is a rapid stabilization of the variables at the remaining nodes. In contrast, at node 12, which houses the Peruvian generator, there is a noticeable increase in the variation, leading to a longer stabilization period compared to the other nodes.

3.3 Opening of Termogas Machala Generator:

To evaluate this event, we used PowerWorld, with the input parameters shown in Figure 34.

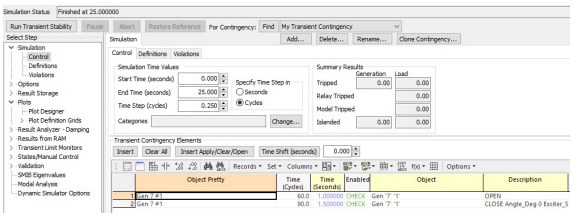

Fig. 34: Event 2 entry in the software

Figure 35 shows the frequency oscillations of two electrical buses after a disturbance. The frequencies shown in orange and purple show a transient response that finally stabilizes after about 8 seconds, reaching a steady state near 60 Hz.

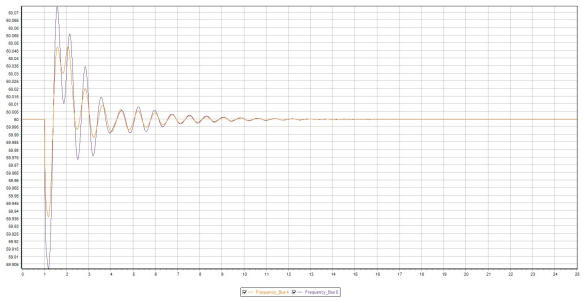

Fig. 35: Frequency at nodes 4 -5

Figure 36 show the frequency of bus 6, bus 7 and bus 8 after a disturbance. All three waveforms exhibit damped oscillations and ultimately converge to a constant frequency of approximately 59,995 Hz, demonstrating the stability of the power system after the initial disturbance.

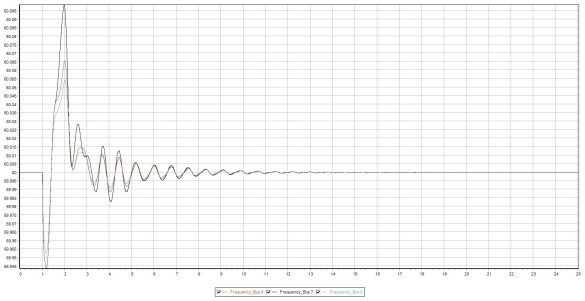

Fig. 36: Frequency at nodes 6 -7 - 8

Figure 37 shows the frequency variations of bus 9, bus 10, bus 11 and bus 12 after a disturbance. The waveforms show damped oscillations and finally converge around 59.995 Hz. This suggests that, despite the initial disturbance, the power grid maintains a constant frequency.

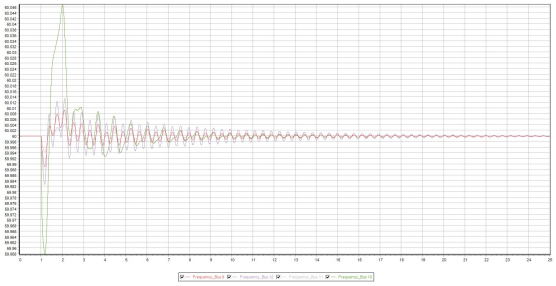

Fig. 37: Frequency at nodes 9 -10 -11-12

The data indicate that the generator output leads to a decrease in frequency. This is influenced by the speed controllers and, after reconnection of the generator, the frequency will stabilize towards the end of the analysis period.

In addition, to confirm the operation of the voltage regulators through the drive system, the variations of the voltages at the nodes are shown in Figure 38.

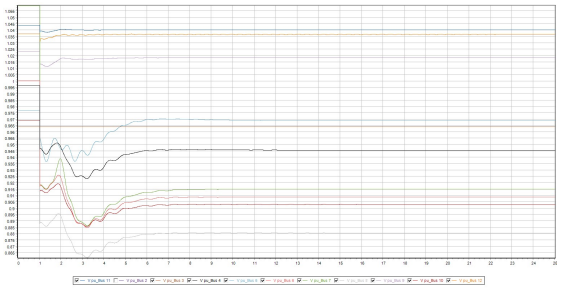

Fig. 38: Node voltages

Figure 38 shows the role of the voltage regulators in mitigating the fluctuations of this electrical parameter throughout the analysis period, thus validating the effectiveness of the exciter models. In the analysis scenario, nodes 4 to 10 show the most notable voltage variation, in agreement with expectations.

To evaluate the voltage and angle stabilization for each node, visual representations are provided in the following shows Figure 39, Figure 40, Figure 41, Figure 42 and Figure 43.

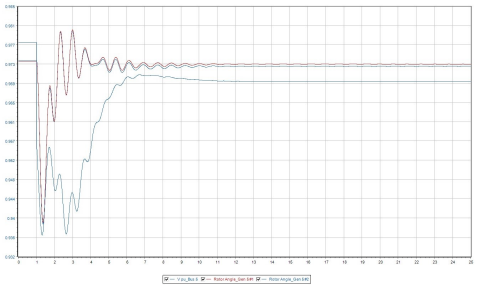

Fig. 39: Voltage and rotor angle variation - node 5

Figure 40 shows the progression of the generator 7 rotor angle and bus voltage 7 after a disturbance. The rotor angle exhibits oscillations before reaching a steady state, while the bus voltage represents an initial decrease followed by a recovery.

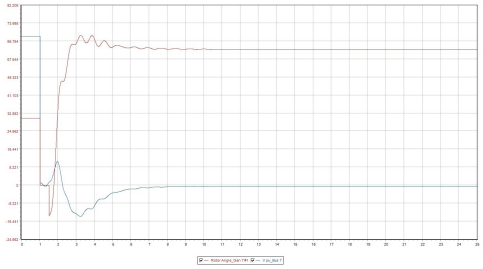

Fig. 40: Voltage variation and rotor angle - node 7

Figure 41 shows the changes in tension and angle of the bus 9 after a disturbance. Initially, the tension shows a decrease, leading to subsequent oscillations before reaching a steady state. Meanwhile, the stress angle undergoes an increase before stabilizing, accompanied by small variations.

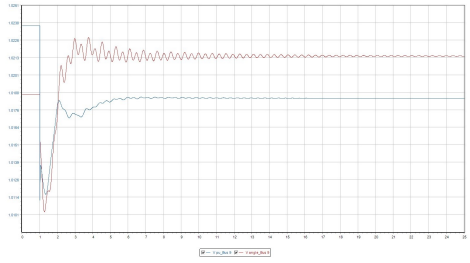

Fig. 41: Voltage variation and rotor angle - node 9

Figure 42 shows the generator rotor angle 11 and the bus voltage 11 after a disturbance. The rotor angle shows an increase with oscillations before reaching a steady state, while the voltage shows a slight decrease before stabilizing with minor oscillations.

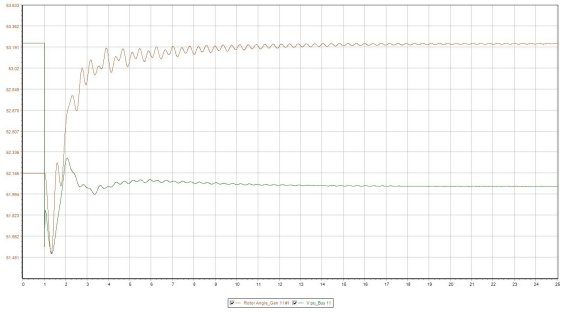

Fig. 42: Voltage variation and rotor angle - node 11

From the voltage and angle variations in each node, it can be seen that except for node 12, in the other nodes there is a stabilization of the variables in a quick way; however, in node 12, where the Peru generator is located, it is again evident that there is a greater variation and its stabilization takes longer than in other busbars. This is shown in Figure 43.

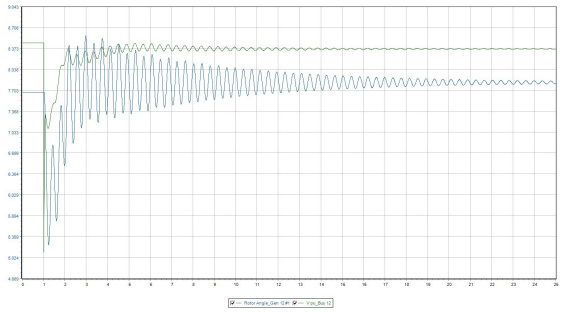

Fig. 43: Voltage variation and rotor angle - node 12

Figure 44 shows the oscillations in the active (MW) and reactive (Mvar) power of a generator after a disturbance. Both parameters before finally reaching a steady state: the MW stabilizes at a constant level and the Mvar shows a more variable stabilization.

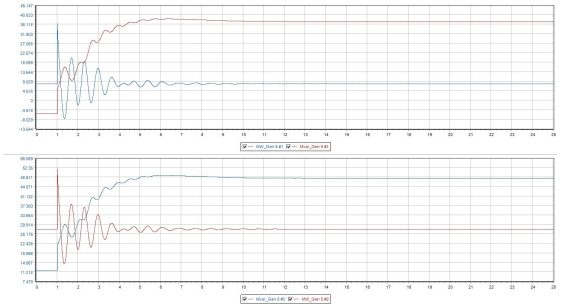

Fig. 44: Variation of P and Q - Generators located at node 5

Figure 45 shows the transient response of the active (MW) and reactive (Mvar) power of a generator after a disturbance. The active power (MW) experiences a sudden decrease before stabilizing, while the reactive power (Mvar) experiences a rapid increase followed by oscillations before reaching a steady state.

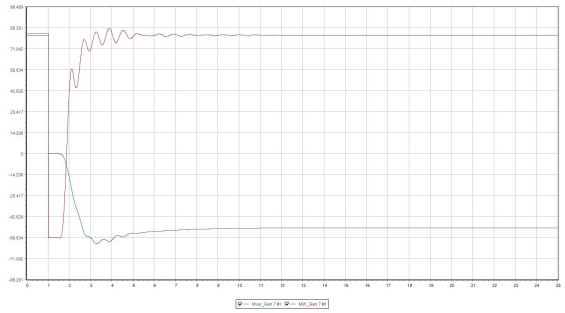

Fig. 45: Variation of P and Q - Generator located at node 7

Figure 46 shows the transient oscillations of the active (MW) and reactive (Mvar) power of generator 11 after a disturbance. Initially, both MW and Mvar experience oscillations before reaching a near steady state.

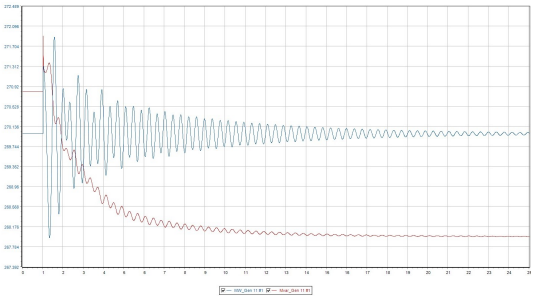

Fig. 46: Variation of P and Q - Generator located at node 11

It has been found that the variations of P and Q at each node indicate that, except at node 12, there is a stabilization of the parameters at a rapid rate at the rest of the nodes. At node 12, which houses the Peru generator, a noticeable increase in variation is observed, leading to a longer stabilization process than at the rest of the nodes, as shown in Figure 47.

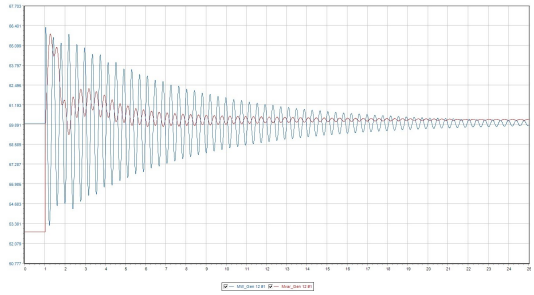

Fig. 47: Variation of P and Q - Generator located at node 12

4 Discussion of Results

The evaluation of transient stability within the southern segment of Ecuador's SNI has revealed several critical weaknesses that could profoundly affect its reliability during transient disturbances, such as faults or variations in load. This evaluation is essential because transient stability is a determinant of the system's capacity to maintain synchronism and revert to normal operational states following a disturbance.

The steady-state simulation of the network indicated that the linkages between the 230 kV Milagro substation and the Guayas - Los Ríos CNEL are presently functioning at 83.5% of their designed capacity. This elevated level of utilization signifies congestion within these lines, which contributes to diminished voltage levels, recorded at 0.9057 pu. Such a voltage level is approaching the minimum operational threshold, highlighting the urgent need for infrastructure enhancements to alleviate congestion, increase capacity, and ensure stable voltage levels throughout the network.

In the course of simulating a three-phase fault on the line connecting nodes 1 and 11, it was noted that the nodes nearest to the fault experienced the most substantial frequency fluctuations. Nonetheless, these fluctuations were adeptly managed by the speed regulators of the generators, which worked to mitigate the effects and stabilize the frequency across the majority of nodes. Despite the rapid stabilization of most segments of the network, node 12, which is linked to a generator from Peru, displayed more pronounced frequency variations and required a longer period to stabilize. This phenomenon indicates a specific vulnerability in the connection with the Peruvian generator, potentially attributable to weaker coupling or less effective control mechanisms at this node. Moreover, the disconnection of the Termogas Machala generator, a critical power source in the region, led to an immediate decline in system frequency. Although the frequency stabilized upon the generator's reconnection, this incident resulted in observable impacts on voltage levels at several adjacent nodes. Most of these nodes rapidly restored their voltage levels, with the exception of node 12, which once again exhibited signs of instability, further highlighting its susceptibility to disturbances.

It is advisable that supplementary protective measures be instituted at node 12. This could involve enhancing control systems, installing more robust protective relays, or strengthening the infrastructure at this site to better manage such disturbances. These enhancements are imperative to fortify the overall reliability of the southern segment of the SNI, ensuring a stable and secure power supply to

the impacted regions, particularly during periods of stress or transient disturbances. Strengthening nodes such as node 12 will aid in preventing localized instabilities from escalating into larger system-wide challenges, thereby preserving the integrity of Ecuador's electrical grid.

5 Conclusion

Based on the findings of the study, conclusions will be developed within the technical domain.

- Stability assessments performed on a segment of the electrical system in Ecuador have identified vulnerabilities and critical points that could jeopardize the reliability and security of the system. These assessments play a vital role in predicting potential problems and implementing appropriate preventive actions.
- It is crucial to put in place sufficient protective measures to address the risks identified in the stability assessments. Specifically, emphasizing the need to introduce customized safeguards to isolate the connection with Peru, as there is an accumulation of vulnerabilities in that particular node. This action will help preserve the integrity of the power grid and prevent possible negative impacts of transient events.
- The results of the analyses suggest that the control systems, operating at both the exciter and speed levels, are effectively performing their function of ensuring power system stability. This determination underscores the efficiency of the current control systems and their ability to maintain operational stability within acceptable limits under regular and transient circumstances.
- Stability analyses provide a solid foundation for continuous improvement of the power system in Ecuador. By identifying areas in need of improvement and opportunities for rationalization, interventions and reinforcement tactics can be implemented to improve the resilience and reliability of the entire system. This forward-looking approach plays a crucial role in ensuring a safe energy supply.

Acknowledgment:

I would like to express my gratitude to Engineer Carlos Quinatoa. To the research assistants Luis Camacho and Jimmy Vaca. Thank you all very much.

Statement:

During the preparation of this work the authors used Grammarly for language editing. After using this service, the authors reviewed and edited the content as needed and take full responsibility for the content of the publication.

References:

[1] J. Constante, A. Riofrío, A. B. D. L. Torre, and J. C. Cepeda, "Methodology for stationary and dynamic modeling of the s.n.i. in hypersim, application of the model in electromagnetic transient analysis for 500 kv systems," *Requirements Engineering*, vol. 16, no. 2, pp. 40–49, 2020.

[2] C. Gallardo and D. Andagoya, "Angular Stability Analysis of the Ecuadorian Electric System," *Escuela Politécnica Nacional, Facultad de Ingeniería Eléctrica y Electrónica*, vol. 33, no. 3, p. 11, 2014.

[3] G. Rodríguez, M. Mulas, S. Loaiza, M. Del Pilar Villalta Echeverria, A. A. Yanez Vinueza, E. Larreta, and L. Jordá Bordehore, "Stability Analysis of the Volcanic Cave El Mirador (Galápagos Islands, Ecuador) Combining Numerical, Empirical and Remote Techniques," *Remote Sensing*, vol. 15, no. 3, pp. 732–732, 2023.

[4] A. S. Kumar, T. Cermak, S. Misak, and B. Horak, "Modeling and simulation for 1.2 kW PEM fuel cell power generation of isolated load conditions," in *2015 International Conference on Electrical Drives and Power Electronics, EDPE 2015 - Proceedings*, (Tatranska Lomnica, Slovakia), pp. 235–240, Institute of Electrical and Electronics Engineers Inc., nov 2015.

[5] N. Hashim, N. Hamzah, M. F. A. Latip, and A. A. Sallehhudin, "Transient Stability Analysis of the IEEE 14-Bus Test System Using Dynamic Computation for Power Systems (DCPS)," in *2012 Third International Conference on Intelligent Systems Modelling and Simulation*, (Kota Kinabalu, Malaysia), pp. 481–486, 2012.

[6] A. A. Fouad, K. C. Kruempel, V. Vittal, A. Ghafurian, K. Nodehi, and J. V. Mitsche, "Transient Stability Program Output Analysis," *IEEE Transactions on Power Systems*, vol. 1, no. 1, pp. 2–8, 1986.

[7] M. Althoff, M. Cvetković, and M. Ilić, "Transient stability analysis by reachable set computation," in *2012 3rd IEEE PES Innovative Smart Grid Technologies Europe (ISGT Europe)*, (Berlin, Germany), pp. 1–8, 2012.

[8] T. Aschenbruck, W. Esterhuizen, and S. Streif, "Transient stability analysis of power grids with admissible and maximal robust positively invariant sets," *at - Automatisierungstechnik*, vol. 68, no. 12, pp. 1011–1021, 2020.

[9] Y. Xu, Y. Chi, and H. Yuan, *"Transient Stability Constrained Optimal Power Flow (TSC OPF)"*, pp. 65–77. Wiley-IEEE Press, 1 ed., 2023.

[10] N. A. Salim, H. Mohamed, M. E. S. Bin Ensnat, and Z. M. Yasin, "System Transient Stability Due to Various Contingency Using Power World Simulator," in *2023 IEEE 3rd International Conference in Power Engineering Applications (ICPEA)*, (Putrajaya, Malaysia), pp. 279–284, 2023.

[11] G. Rawat and S. Chauhan, "Transient Stability Analysis of Wind Farm Integrated Power Systems using PSAT," in *2023 Second International Conference on Electrical, Electronics, Information and Communication Technologies (ICEEICT)*, (Trichirappalli, India), pp. 1–8, 2023.

[12] S. Gu, J. Qiao, Z. Zhao, Q. Zhu, and F. Han, "Power System Transient Stability Assessment Based on Graph Neural Network with Interpretable Attribution Analysis," in *2022 4th International Conference on Smart Power & Internet Energy Systems (SPIES)*, (Beijing, China), pp. 1374–1379, IEEE, 2022.

[13] R. Reinoso and C. Toaquiza, "Transient Stability Analysis in Multi-machine systems considering AVR control in DIgSILENT's PowerFactory software," *Ciencias de la Ingeniería y Aplicadas*, vol. 7, no. 1, pp. 11–25, 2023.

[14] L. Arcos and I. Flores, *"Transient stability analysis of the national interconnected system of Ecuador"*. Thesis, Escuela Politécnica Nacional, 2007.

[15] J. Weber, *Description of Machine Models GENROU, GENSAL, GENTPF and GENTPJ*. PowerWorld Corporation, 2001 South First Street, Champaign, IL 61820, October 22, 2015 (December 3, 2015 corrections) 2015. Director of Software Development.

[16] M. Monagas, Eva Palacios, Bincer Rueda, "Transient stability analysis of an electric power generation and transmission system. Case: Electricity of Valencia-Corpoelec," *Revista INGENIERÍA UC*, vol. 17, no. 3, pp. 57–67, 2010.

[17] P. Corporation, *"Exciter and Governor Modeling"*. PowerWorld Corporation, 2001 S. First St, Suite 203, Champaign, IL 61820, 2020. Accessed: 2024-07-17.

[18] J. F. Quisilema-Quiñaluisa, "Analysis of transient stability in electrical power systems by the Runge-Kutta method," *Revista Vínculos*, vol. 18, no. 1, pp. 64–71, 2021.

[19] National Energy Control Center (CENACE), "Cenace library." `https://www.cenace.gob.ec/biblioteca/`. Accessed: 2024-07-03.

[20] Agency for Regulation and Control of Energy and Non-Renewable Natural Resources, "Electricity sector statistics." `https://www.controlrecursosyenergia.gob.ec/estadistica-del-sector-electrico/`. Accessed: 2024-07-03.

[21] Ministry of Energy and Non-Renewable Natural Resources, "Resources and energy geoportal." `https://geoportal.controlrecursosyenergia.gob.ec/`. Accessed: 2024-07-03.

[22] Agency for Regulation and Control of Energy and Non-Renewable Natural Resources, "Regulation no. arcernnr-004/20 (codified): Operational planning, dispatch and operation of the electric power system." `https://www.controlrecursosyenergia.gob.ec/estadistica-del-sector-electrico/`, 2020. Accessed: 2024-07-03.

Contribution of Individual Authors to the Creation of a Scientific Article (Ghostwriting Policy)

Each author contributed to the creation of the scientific article, Engineer Carlos Quinatoa and myself Darwin Pila led the research and data . Luis Camacho and Jimmy Vaca helped with the manuscript and critically reviewed the content.

Sources of Funding for Research Presented in a Scientific Article or Scientific Article Itself

No funding was received for conducting this study.

Conflicts of Interest

The authors state that they have no financial interests or personal relationships that could affect the work done in this study.